

HIGH PERFORMANCE THIN FILM MAGNETS

S. FÄHLER, V. NEU, M. WEISHEIT, U. HANNEMANN, S. LEINERT, A. SINGH, A. KWON,
S. MELCHER, B. HOLZAPFEL, AND L. SCHULTZ
IFW Dresden, Helmholtzstraße 20, 01069 Dresden, Germany
Corresponding author e-mail: s.faezler@ifw-dresden.de

Abstract

The growth of highly textured, highly coercive Nd-Fe-B, Sm-Co and FePt films on heated substrates prepared by pulsed laser deposition is summarized. When prepared under optimum conditions, these films can exhibit very high coercivities of 2.0 T for Nd-Fe-B, 3.6 T for Sm-Co, and 5.6 T for FePt, while differing significantly in texture, microstructure, morphology and coercivity mechanism. The feasibility of these three systems for applications in microelectromechanical systems (MEMS) and as recording media is discussed.

Introduction

Hard magnetic films are required for applications in magnetic microelectromechanical systems (MEMS) and as data storage media. Both applications require better materials. For MEMS the aim is to provide high power at reduced dimensions, in recording media the challenge is to avoid a loss of information due to the superparamagnetic limit, where the magnetisation switches by thermal activation when the grain size drops below a critical length. Therefore, materials with a higher magnetocrystalline anisotropy are required for a further increase of bit density.

The basis for high performance magnetic films is the choice of material. The intrinsic properties and the resulting extrinsic magnetic properties of several hard magnetic materials are summarized. We then review different preparation routes applied to the deposition of Nd-Fe-B, Sm-Co and FePt films. As most high performance applications require a texture of the easy axis along the application direction, the necessary conditions to achieve the desired uniaxial texture are discussed. The focus will be on the temperature treatment, as a crucial parameter influencing phase formation, texture and microstructure. For each system prepared at the optimum conditions the microstructure and related coercivity mechanism will be discussed. As a summary an extended discussion on the suitability of these materials for various applications will be given.

1 Material properties

For applications the films must exhibit good extrinsic hard magnetic properties. For MEMS - as in bulk magnets - the key property is the energy density $(BH)_{max}$ describing the maximum energy which can be stored in a magnet. The theoretical maximum energy product $(BH)_{th,max}$ achievable in textured magnets is determined by the intrinsic properties of the material and scales with the square of the saturation magnetisation polarization J_S , provided that the anisotropy field $\mu_0 H_A$ is sufficiently high. For maximum energy product, the coercivity $\mu_0 H_C$ (which hardly exceeds 1/3 of the anisotropy field) has to be higher than half of the remanence J_R . The commonly used high performance magnets based on rare earth - transition metal alloys as well as the group of the ferromagnetic $L1_0$ phases fulfill these criteria (table 1). Compared to ferrites and Co, which are also discussed for MEMS, they exhibit a significantly higher magnetocrystalline anisotropy. The FePt $L1_0$ phase is ranked between Nd-Fe-B and Sm-Co when considering $\mu_0 H_A$ and J_S and is the best of the ordered $L1_0$ phases.

Nd-Fe-B has the highest theoretical maximum energy product $(BH)_{th,max}$, resulting from the high saturation magnetization. Bulk magnets come close to that value [1]. Next comes $L1_0$ ordered FePt, known since the 1930s, but the significantly higher material costs prohibit the widespread use in bulk magnets. Sm-Co is used in bulk form for high temperature applications due to its high Curie temperature.

Table 1 *Intrinsic and derived properties of various hard magnetic materials [2,3,4,5]: T_C Curie temperature, K_U uniaxial magnetocrystalline anisotropy constant, J_S saturation polarization, $\mu_0 H_A$ anisotropy field, $BH_{th,max}$ theoretical maximum energy product (* For Co, $BH_{th,max}$ is not achievable, as $\mu_0 H_C < \mu_0 H_A < 0.5 J_S$), D_P critical diameter for the superparamagnetic limit [6].*

Material	T_C (K)	K_U (10^6 J/m ³)	J_S (T)	$\mu_0 H_A$ (T)	$BH_{th,max}$ (kJ/m ³)	D_P (nm)
Nd ₂ Fe ₁₄ B	585	4.6	1.60	7.3	512	3.7
Sm ₂ Co ₁₇	1173	3.5	1.25	7	326	4.1
Sm ₂ Co ₇	693	6.3	0.8	20	127	3.4
SmCo ₅	1000	11-20	1.14	24-44	258	2.7-2.2
L1 ₀ FePt	750	6.6-10	1.43	11.6	407	2.8
L1 ₀ CoPt	840	4.9	1.00	12.3	199	3.6
L1 ₀ FePd	760	0.7-2.4	1.38	3.3	379	5.1
Hex. Co ₃ Pt	1100	0.8-2	1.38	3.6	378	4.8
BaO·6[Fe ₂ O ₃]	450	0.3	0.5	1.2	50	9.4
Co	1117	0.45	1.79	0.6	*	8

The miniaturization of MEMS has reached a point where thinning of bulk samples becomes less efficient compared to the deposition of thick films (of the order of some μm).

On the background of continually increasing area density in magnetic data storage since the middle of the nineties a lot of effort has been put into the development of thin hard magnetic films. With increasing miniaturization the material costs take a minor role compared to process costs, and, therefore, the interest in FePt and related systems increased. In magnetic data storage the area density follows Moore's law and doubles every 12-18 months. This requires a shrinkage of the bit and therefore grain size. Today's media exhibit grain sizes below 10 nm, a size close to the limit when thermal fluctuations are sufficient to switch magnetisation in conventional media based on Co and result in a loss of data. The critical grain diameter D_P describing the superparamagnetic limit mostly depends on the magnetocrystalline anisotropy. Within magnetic media applications the anisotropy becomes, therefore, more important than J_S . Sm-Co exhibits the highest anisotropy, resulting in the smallest critical grain size. For reduced noise, recording media requires a texture of the easy axis, which should lie in-plane for conventional longitudinal media and perpendicular to the substrate in the case of perpendicular recording.

2 Experimental

Films were deposited in a UHV chamber (base pressure $< 10^{-9}$ mbar) using pulsed laser deposition (PLD). A KrF laser beam (248 nm, 25 ns) was directed by a mirror/lens system into the vacuum chamber and an aperture in the beam line was imaged onto the targets resulting in an homogeneous energy density of about 5 J/cm². Elemental targets were alternately moved into the laser beam to deposit films with the desired composition. As some soft magnetic Fe or Co droplets are deposited together with the hard magnetic film, sometimes a low field shoulder in the hysteresis loops can be observed. The target-to-substrate distance was typically 40 mm. Prior to film deposition, the deposited mass per pulse was measured for each target with an Inficon XTM/2 rate monitor. The substrate temperature was monitored with an Impac IGA 120 pyrometer. A 100 nm thick Ta buffer layer was deposited on the heated sapphire substrate prior to the Nd-Fe-B film deposition, for the

Sm-Co films a Cr buffer was used. FePt was deposited directly on MgO substrates. To prevent oxidation of the films, Nd-Fe-B and Sm-Co films were covered in-situ with a 30 nm Cr layer at a temperature below 250°C. Details are published elsewhere [7].

Microstructural investigations were performed with a Digital Instruments Dimension 3100 AFM in tapping mode. X-ray q - $2q$ scans were measured with a Siemens D5000 diffractometer using Co K_α radiation. The magnetic properties were measured with a Quantum Design ACMS P500 in dc mode and a Quantum Design VSM.

3 Nd-Fe-B films

The magnetic material which dominates the high performance bulk magnets market – $\text{Nd}_2\text{Fe}_{14}\text{B}$ – has been deposited for some years now with a sufficient quality to be attractive as a magnetic film [8-15]. When deposited on appropriate heated substrates these films possess a good magnetic texture with the easy magnetization axis perpendicular to the substrate and coercivities of 1 T and above.

Here we show films deposited on epitaxial Ta (110) buffers deposited on Al_2O_3 single crystal substrates. Ta proved to be more inert than the commonly used Cr [16]. In fig. 1 the influence of the substrate temperature on coercivity, remanence and magnetic texture is shown. Below 550°C the temperature is too low for the formation of the $\text{Nd}_2\text{Fe}_{14}\text{B}$ phase, above 650°C interdiffusion and the formation of unwanted phases result in a degradation of coercivity and magnetization (for more details see [17]). At a medium temperature around 630°C a very high degree of magnetic texture (quantified by the very low in-plane to out-of-plane remanence ratio) and a high coercivity up to 2 T can be obtained. This is the result of an epitaxial growth with an almost perfect c-axis alignment of all crystallites perpendicular to the film plane, as we showed recently [18]. The intrinsic properties (anisotropy field and spin reorientation transition) of these films are comparable to bulk samples. The high coercivity of up to 2 T is obtained by a granular growth on the non-wettable Ta substrate [19]. As seen in Fig. 2, the epitaxial growth results in partly isolated, rectangular shaped grains reflecting the tetragonal $\text{Nd}_2\text{Fe}_{14}\text{B}$ unit cell. In addition to that, the domain structure in the remanent state as measured with an MFM is depicted in fig. 2. Stripe domains are observed as expected for a film with a perpendicular magnetic anisotropy. The dependence of the stripe domain width on the thickness of the grains can be understood with domain theory of extended films [17]. As the isolated grains exhibit a quite regular habitus with little defects, nucleation of reversed domains can be avoided resulting in the high coercivity [18]. This can also be seen in the high initial susceptibility of the virgin magnetization curve (insert in fig. 1).

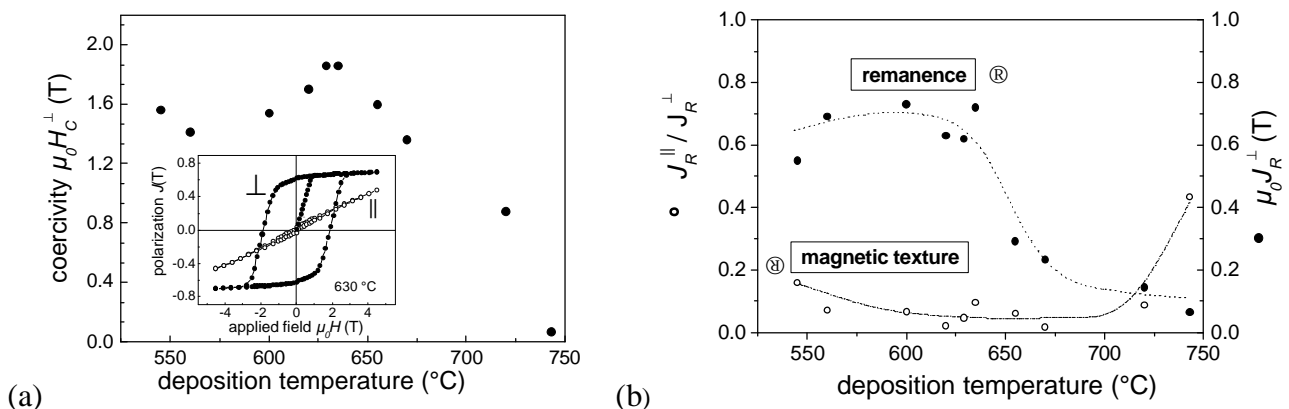


Figure 1 Extrinsic magnetic properties of Nd-Fe-B films as a function of deposition temperature. (a) coercivity measured perpendicular to the plane (\perp). The insert shows a hysteresis for the optimum deposition temperature of 630°C. (b) Remanence measured perpendicular to the plane and magnetic texture described by the in-plane (\parallel) to out-of-plane (\perp) remanence ratio.

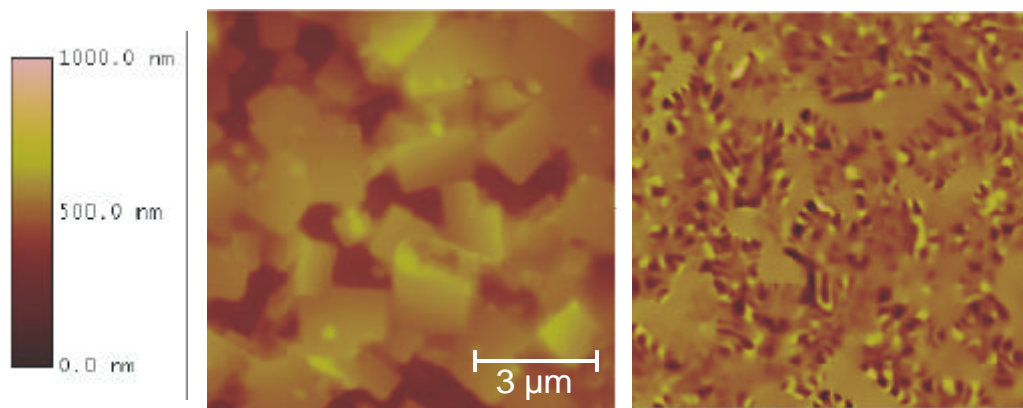


Figure 2: Topography (left) and magnetic contrast as measured by MFM (right) for a Nd-Fe-B film deposited at 630°C. Stripe domains and edge effects are clearly visible.

Oxidation can introduce defects at the surface. This does not modify the overall intrinsic magnetic properties (like $\mu_0 H_A$ and J_S), but the coercivity drops significantly within some hours after deposition as the oxidized surface introduces nuclei for domain reversal [20]. The mentioned coverage with a Cr protection layer is, therefore, inevitable for long term stability.

For this growth a relatively high Nd content is necessary, which results in a significantly lower remanence than obtained in bulk magnets [17].

When comparing these films with those prepared by other groups, one may consider these films to be optimized with respect to texture and coercivity at the expense of saturation magnetization and roughness. The increase of coercivity with higher Nd content is well known from bulk magnets and thin films [21]. Also, a strong correlation of coercivity and roughness is observed often [9] (but not always reported).

As the microstructure obtained by the granular growth makes it difficult to scale up the film thickness, post-annealing of cold deposited films is an alternative. With this processing route, typically isotropic, but smooth films can be prepared and an increase of remanence above half the saturation magnetization can be obtained by exchange coupling [22].

Another approach can combine the two above mentioned methods [23]. The deposition of Nd-Fe-B at an intermediate temperature around 400°C is followed by a post-annealing step. Due to this procedure, a good texture in combination with a high coercivity is obtained [23, 24]. Currently it is not clear whether the texture evolves by the growth of small oriented nuclei created during the first deposition step [23-25] or by a directed crystallization originating at an interface [26-28]. Recent advances can be found in the contribution of Kornilov in these proceedings.

4 Sm-Co films

The Sm-Co system contains various highly anisotropic phases, which are likewise interesting for thin film applications (table 1). The main difference to Nd-Fe-B films is the typically observed planar magnetic texture, where the c-axis (the easy magnetization axis) lies in the film plane. These films are therefore applicable when strong permanent magnetic fields in the film plane are needed. Furthermore, these phases grow at rather moderate temperatures above 350°C, which is of benefit for preparation and film smoothness.

The known drawback of Sm-Co is the moderate saturation magnetization of at most 1.25 T for $\text{Sm}_2\text{Co}_{17}$, and hence, besides coercivity, the degree of texture is of vital importance for optimum magnetic performance. We distinguish between the preparation of films on untextured substrates, which leads to a Sm-Co fiber texture, and the deposition on appropriate buffer, where epitaxial growth is possible. In the first case, Sm-Co films are deposited on Si substrates with an amorphous SiN top layer and an additional Cr buffer layer. The typical planar magnetic texture develops upon direct crystallization on the heated substrate, however, there is only a random distribution of the easy

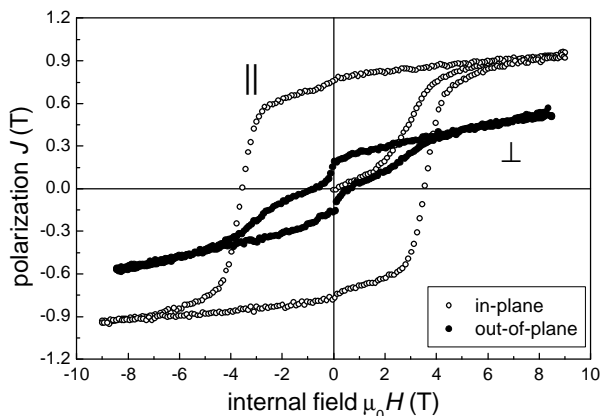


Fig. 3: Hysteresis of a 70 nm thick SmCo_5 film grown on a SiN/Si substrate using a Cr buffer. Polarization was measured parallel (in-plane) and perpendicular (out-of-plane) to the film plane.

axis within the film plane. The maximum remanence achievable in these films is 64% of the saturation, assuming no out-of-plane component for the c-axes. In the second case, the Sm-Co is deposited on MgO (100) single crystal substrates with a Cr (100) buffer layer. Both, Cr and Sm-Co grow epitaxially, and for optimum deposition conditions the Sm-Co easy axis is only oriented along the MgO [100] and [010] directions.

4.1 Textured Sm-Co

The growth of textured SmCo_5 or SmCo_7 films on untextured substrates has been pioneered by Cadieu [29], and the deposition by magnetron sputtering is established for MEMS[30]. These films have excellent hard magnetic properties, which can be largely tailored by the Sm-Co stoichiometry [31]. Coercivities reach values of up to 1.8 T when measured in the film plane.

The magnetic texture is often quantified by the remanence ratio J_R^\perp/J_R^\parallel and can be as low as 0.05. More recently, pulsed laser deposition has been used to prepare textured Sm-Co films [32-34]. Due to the high instantaneous deposition rates inherent of the UHV-PLD process, the grain size is rather small, the films are smooth and high coercivities are achieved. Here we present our recent improvements in the preparation of Sm-Co films by varying the deposition condition applied in the pulsed process. A 30 nm thick Cr buffer layer is deposited on a heated SiN/Si substrate. The texture of the Cr layer varies with increasing substrate temperature from a predominantly (110) fiber texture to a Cr (100) fiber texture. As a (100) texture was found to be beneficial for the subsequent textured growth of Sm-Co, the Cr buffer is deposited at a high temperature of 630°C [35]. The SmCo_5 film was deposited at 460°C on top of the Cr buffer and grows with a predominant (110) fiber texture. As we use deposition from elemental targets, the targets are changed repeatedly after a few pulses and the complete film is composed of several sublayers with nominal SmCo_5 composition. The thickness of this sublayer plays an important role in determining the diffusion length and consequently influences the phase formation. By reducing the nominal sublayer thickness from typically 1 nm down to 0.15 nm, both, sharpness and intensity of the Sm-Co (110) and (220) x-ray reflections increased significantly. At the same time coercivity and the degree of texture improve considerably. We attribute this to the better element mixing and therefore a shorter required diffusion path which results in an improved phase formation. With this process extraordinarily good hard magnetic properties are obtained (Fig. 3). The film possesses an open, square shaped hysteresis with a coercivity of $\mu_0 H_c^\parallel = 3.6$ T when measured in the film plane. The quite low susceptibility at the beginning of the virgin curve suggests that coercivity in these films could be controlled by pinning. The out-of-plane loop is narrow and flat resulting in a low remanence ratio of only 0.15. This very well textured film has a considerably higher coercivity than ever reported for a likewise textured Sm-Co film prepared on a non-textured substrate. We attribute this to the good phase formation due to an

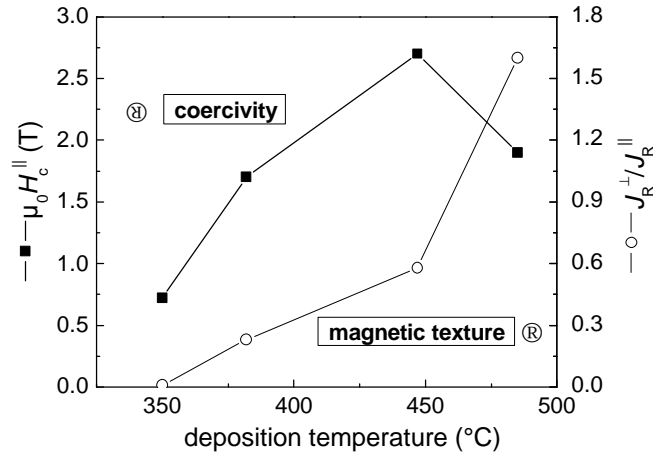


Figure 4: Influence of deposition temperature on coercivity measured in-plane and magnetic texture described by the out-of-plane to in-plane remanence ratio of Sm_2Co_7 films grown on an epitaxial Cr(100) buffer on MgO(100).

optimized deposition procedure, small grain sizes due to the high instantaneous deposition rates inherent of the PLD process, and high purity deposition conditions due to the preparation under UHV [7].

4.2 Epitaxial Sm-Co

Epitaxial growth has so far only been attempted for Sm-Co films with nominal Sm_2Co_7 composition by magnetron sputtering [36]. When prepared on MgO (100) substrates, a Cr (100) buffer layer grows epitaxially with Cr[100] || MgO[110]. The good lattice match between the Cr (100) surface and the Sm_2Co_7 (110) lattice plane leads to an epitaxial growth of Sm-Co on Cr with Sm-Co[001] || Cr[110]. Due to the fourfold symmetry of the Cr surface this corresponds to two orthogonal directions of the Sm-Co c-axis along the substrate edges.

When prepared by PLD, the same epitaxial growth is possible. A 30 nm thick Cr buffer is deposited at 640°C onto MgO(100) single crystal substrates. A 70 nm thick Sm-Co film with nominal composition close to Sm_2Co_7 is deposited at a laser repetition rate of 5 Hz at varying temperatures. Figure 4 shows the coercivity and the remanence ratio for 4 films as a function of the Sm-Co deposition temperature. The in-plane hysteresis was measured along the MgO[100] direction.

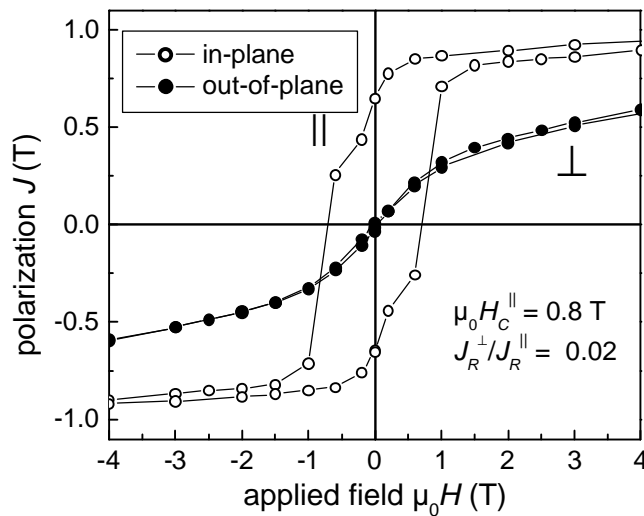


Figure 5: Hysteresis of an epitaxial Sm_2Co_7 film grown on Cr(100)/MgO(100) at 350°C.

The texture of the films depends strongly on the substrate temperature and reveals a crossover from a predominantly out-of-plane texture at higher deposition temperatures to the aimed in-plane texture for low deposition temperatures.

In all cases pole figure measurements reveal an epitaxial growth of the Sm_2Co_7 phase, however, for higher temperature additional texture components are present. At lower deposition temperatures only the above mentioned epitaxial relation is found and consequently the remanence ratio approaches the ideal value of zero. Details of deposition conditions, epitaxial growth and the anisotropy within the film plane will be published elsewhere [37]. Also these Sm-Co films achieve very high coercivity values (up to 2.6 T). The coercivity decreases, however, for the lower deposition temperatures required for perfect texture. Possibly, the high anisotropic Sm-Co phase is not fully formed and the preparation conditions need to be optimized further.

4 FePt films

In order to show the strong temperature dependence of their hard magnetic properties, FePt films with a nominal thickness of 40 nm have been grown at room temperature, at 700°C and at 800°C on MgO(100) substrates. No buffer or cap layer is needed due to the excellent corrosion resistance of FePt. The film deposited at room temperature does not show the superstructure (001) peak of the $L1_0$ ordered phase (see Figure 6). Only the (200) peak is present, indicating a pronounced $(100)_{\text{fcc}}$ texture. For the higher deposition temperature of 700°C this peak broadens into (200)_{fcc} as well as (200) and (002) components of the $L1_0$ ordered phase, i. e. components where the easy magnetization axis lies in the plane and perpendicular to the plane, respectively. Due to the overlap of these peaks, it is not possible to accurately estimate the order parameter, but the presence of the (001) superstructure peak shows that a certain amount of the ordered phase has formed. At a deposition temperature of 800°C only the $L1_0$ (002) component forms, i. e. a pure perpendicular texture of the easy axis. The (002) orientation is favored because of the lower lattice mismatch of the a-axis to the MgO(100) surface (8%) compared to the c-axis (12%). The intensity ratio of the (001) to the (002) peak indicates nearly complete chemical order.

The surface morphology of the films changes from smooth for the room temperature deposited film to granular for the high temperature films (Figure 7) due to the positive interface energy between FePt and MgO. The grain size of the film deposited at 700°C is smaller and the grains are more connected than in the 800°C film, where the grains are more regular and perfectly isolated from

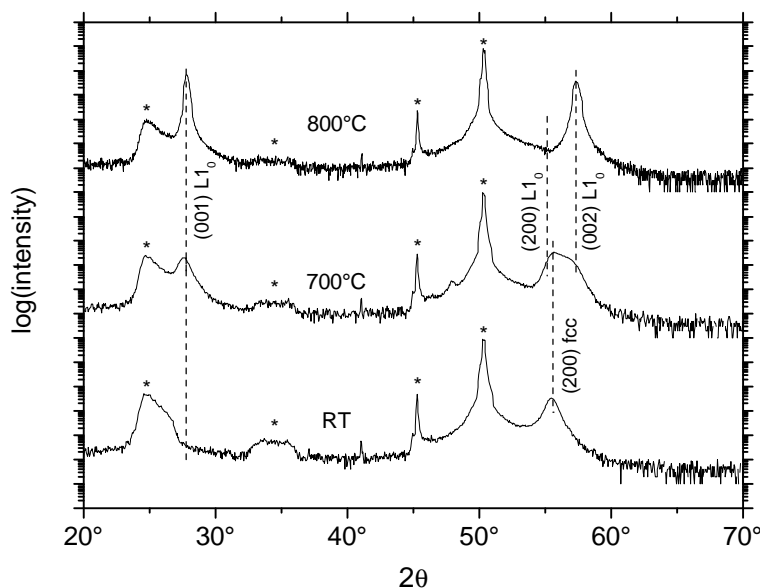


Fig. 6: X-ray diffraction patterns for FePt films deposited at room temperature, 700°C and 800°C on MgO(100). Substrate peaks are marked with an asterisk (*).

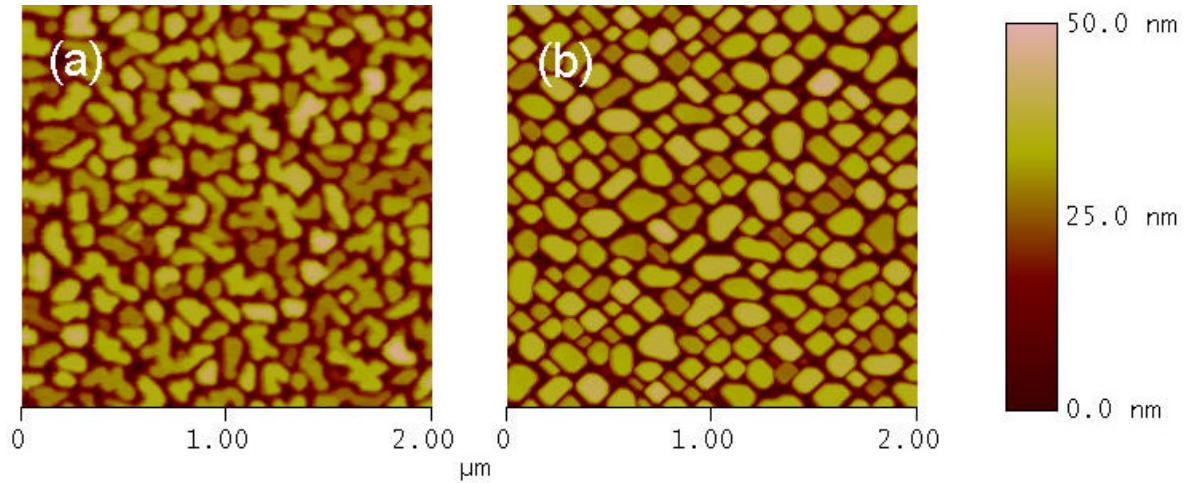


Fig. 7: AFM surface morphology of FePt deposited at 700°C (a) and 800°C (b)

each other. The smaller grains have rectangular shape with their edges oriented along the $\langle 110 \rangle$ directions of the substrate, indicating epitaxial growth.

The combination of nearly complete ordering, strong perpendicular texture of the easy axis and isolated, weakly interacting grains results in strong perpendicular magnetic anisotropy and excellent hard magnetic behavior for the film deposited at 800°C, which has a coercivity of $\mu_0 H_C^\perp = 5.6$ T (Figure 8a). The soft magnetic contribution is a result of pure Fe droplets, which are a byproduct of the PLD process. Reducing the deposition temperature by only 100 K to 700°C leads to a strong degradation of the hard magnetic properties ($\mu_0 H_C = 0.7$ T). Shima et al. have shown that sputtering FePt on MgO(100) at 700°C yields well ordered, hard magnetic films with coercivities of 4 T [38]. The difference to this work might be due to the kinetic energy of the deposited particles (around 100 eV) during PLD compared to 10 eV during sputtering. This causes implantation of the arriving atoms a few nanometers deep into the growing film [39], and the thermodynamically driven ordering process has to compete against this ballistic mixing. Thus higher temperatures, which enable bulk diffusion, are required for complete chemical order. A further decrease of the kinetic energy by using high pressure during sputtering allows a further reduction of preparation temperature [40]. The high temperature required here is in agreement with recently reported data for post-annealed FePt nanoparticles embedded in a C matrix, where maximum order and a correspondingly high coercivity of 3.4 T are obtained after annealing at 800°C [41]. For room temperature deposition, no hard magnetic behavior is observed due to the complete lack of chemical order (Figure 6).

Figure 8b shows the virgin magnetization curves for the films prepared at the three different

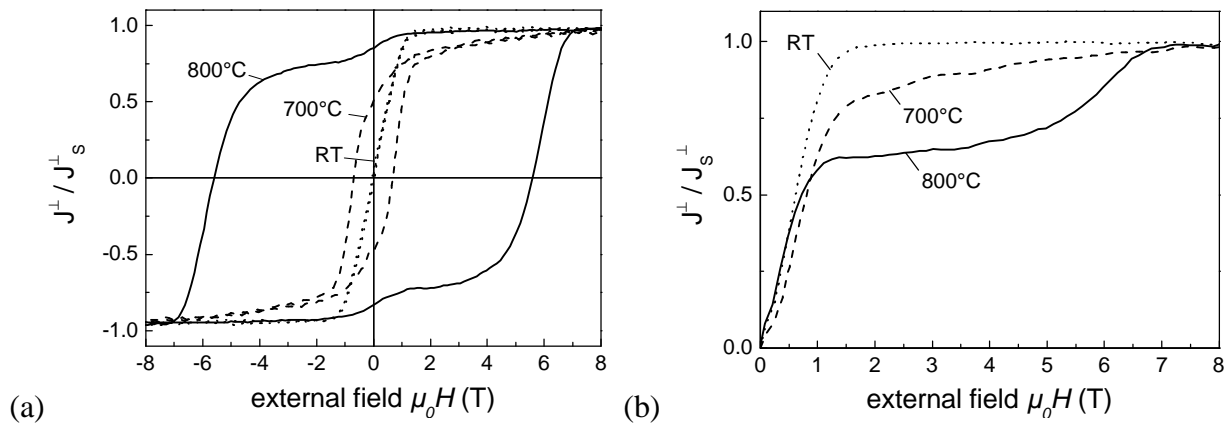


Fig. 8: Out-of-plane hysteresis loops (a) and virgin magnetization curves (b) of 40 nm thick FePt films deposited at room temperature, 700°C and 800°C on MgO(100). The magnetization is given relative to the magnetization at 9 T, which is around 1.0(1) T in all cases. The error is due to the uncertainties in the thickness of the samples.

temperatures. The unusual (or two step) shape observed for the film prepared at 800°C can be explained as follows: The strong increase of magnetization at low applied fields is attributed to domain walls being driven out of the larger grains. Even though the sample is not saturated, the magnetization does not increase appreciably between 1 and 4 T, indicating that single domain grains (presumably the smaller ones) with magnetization opposite to the applied field are still present. These grains switch at fields above 4 T by nucleating a reverse domain. After this first magnetization of the film, all grains are in a single domain state and can switch only at high field by reverse domain nucleation (Figure 8a).

4 Comparison

All three systems allow the preparation of epitaxial films with a very high coercivity. The most striking difference in these systems is the different texture. Nd-Fe-B and FePt films have been grown with the easy magnetization axis perpendicular to the substrate whereas in the case of Sm-Co the easy magnetization axis lies within the film plane. These orientations can not only be obtained on single crystalline substrates, but also on technical substrates with appropriate buffers (MgO for FePt [42], Ta for Nd-Fe-B [43]). L₁₀ FePt can also be grown epitaxial in (100) [44], (101) [45] or (111) [46] orientation. These materials can thus be grown with textures appropriate for most applications.

Another important difference is the microstructure and the related coercivity mechanism. Nd-Fe-B and FePt grow in a granular fashion and the isolated growth allows a magnetic decoupling of the grains. In order to achieve this, high temperatures are necessary for perfect phase formation and regular grains, avoiding domain nucleation at defects. In bulk sintered Nd-Fe-B magnets this is accomplished by an optimized long annealing procedure, but for thin films the high reactivity does not allow a long annealing time [13]. The reason for high coercivities in the Sm-Co films apparently differs strongly from the Nd-Fe-B and FePt samples. Due to small sizes of about 40 nm the individual grains should be in a single domain state for an as-prepared film. The low initial susceptibility (see Fig. 3) resembles the behavior known for small particles that interact only weakly. Additional exchange interactions or the formation of interaction domains via magnetostatic coupling can, however, not be excluded. To which extend such effects play a role in the magnetization behavior and how it differs from the textured to the epitaxial films still needs to be investigated. Since the Sm-Co films are smooth, upscaling of the film thickness is simpler compared to the granular Nd-Fe-B and FePt films. Whereas the granular growth is of benefit for magnetic recording, especially patterned MEMS require smooth, thick films. For MEMS Sm-Co films, post-annealed Nd-Fe-B films or electroplated FePt films [47] are therefore more suitable.

The phase formation of Nd-Fe-B requires a significantly higher temperature than Sm-Co. With FePt an even higher temperature is necessary for very high coercivities, but with optimized growth conditions temperatures below 500°C are enough for a coercivity sufficient for a maximum energy product [40]. A lower preparation temperature reduces the effort of the production process, and reactivity and interdiffusion become less critical in reactive thin films. Here the inert FePt, which does not require buffer or protection layers, has a clear advantage compared to the strongly reactive Nd-Fe-B and modestly reactive Sm-Co. With the reduced size used in magnetic recording, stability is crucial, especially as no thick protection layer can be used which would increase the distance to the read/write head. But also the patterning process of MEMS requires a stable material and new methods to protect the side areas of the patterns.

The application areas for Nd-Fe-B films are thus in thick MEMS, possibly prepared by a two step temperature regime. With a reduced size, the advantage of the low material costs will be overcome by the increasing processing costs and the need for stability. This is motivating the use of new preparation routes like electrodeposition for expensive materials like FePt [47]. As it is hard in thin Nd-Fe-B films to achieve a remanence as high as in bulk materials, Sm-Co and FePt will be more important. When reducing the thickness down to some 10 nm as required for magnetic recording, the higher chemical stability of FePt might be more important than the lower critical grain size possible with Sm-Co.

Acknowledgements

This work was supported by the DFG as part of SFB 463: "Rare earth transition metal compounds: structure, magnetism and transport" and by the DFG project FA 453/1-1

References

- [1] W. Rodewald, B. Wall, M. Katter, K. Uestuener, IEEE Trans. Mag. **39**(5) (2003) 2932
- [2] A. Cebollada, R. F. C. Farrow, M. F. Toney, In: H. S. Nalwa (Ed.): *Magnetic Nanostructures*, ASP, Stevenson Ranch (2002) 931
- [3] T. Klemmer, D. Hoydick, H. Okumura, B. Zhang, W. A. Soffa, Scr. Metal. Mater. **33** (1995) 1793
- [4] R. C. O'Handley, *Modern Magnetic Materials, Principles and Practice*, John Wiley & Sons, Inc.(2000) 485
- [5] D. Weller, A. Moser, IEEE Trans. Mag. **35** (1999) 4423
- [6] D. Weller, A. Moser, L. Folks, M. E. Best, W. Lee, M. F. Toney, M. Schwickert, J. U. Thiele, IEEE Trans. Mag. **36** (2000) 10
- [7] S. Fähler, U. Hannemann, M. Weisheit, V. Neu, S. Melcher, S. Leinert, S. C. Wimbush, A. Singh, A. Kwon, B. Holzapfel, L. Schultz, Appl. Phys. A (2004), in press
- [8] F. J. Cadieu, T. D. Cheung, L. Wickramasekara, N. Kamprath, IEEE Trans. Mag. **MAG-22**(5) (1986) 752
- [9] S. Parhofer, C. Kuhrt, J. Wecker, G. Gieres, L. Schultz, J. Appl. Phys. **83** (1998) 2735
- [10] V. Neu, U. Hannemann, S. Fähler, B. Holzapfel, L. Schultz, J. Appl. Phys. **91** (2002) 8180
- [11] W. Liu, Z. D. Zhang, J. P. Liu, B. Z. Cui, X. K. Sun, J. Zhou, D. J. Sellmyer, J. Appl. Phys. **93** (2003) 8131
- [12] A. Melsheimer, H. Kronmüller, Physica B **299**(3-4)2 (2001) 251
- [13] S. Fähler, U. Hannemann, V. Neu, V. Hoffmann, B. Holzapfel, L. Schultz, 17th Int. Workshop on Rare-Earth Magnets and their Applications; Ed. G. C. Hadjipanayis, M. J. Bonder (Eds.), Rinton Pres, Princeton (2002) 449
- [14] B. A. Kapitanov, N. V. Kornilov, Y. L. Linetsky, V. Y. Tsvetkov, J. Mag. Mag. Mat. **127**(3) (1993) 289
- [15] T. Okuda, A. Sugimura, O. Eryu, L. K. E. B. Serrona, N. Adachi, I. Sakamoto, A. Nakanishi, Jpn. J. Appl. Phys. **42** (2003) 6859
- [16] U. Hannemann, S. Fähler, S. Oswald, B. Holzapfel, L. Schultz, J. Mag. Mag. Mat. **242-245** (2002) 1294
- [17] V. Neu, S. Melcher, U. Hannemann, S. Fähler, L. Schultz, Phys. Rev. B (2004) submitted
- [18] U. Hannemann, S. Fähler, V. Neu, B. Holzapfel, L. Schultz, Appl. Phys. Lett. **82**(21) (2003), 3710
- [19] U. Hannemann, S. Melcher, S. Fähler, V. Neu, B. Holzapfel, L. Schultz, IEEE Trans. Mag. **39**(5) (2003) 2726
- [20] S. Fähler, U. Hannemann, S. Oswald, V. Neu, B. Holzapfel, L. Schultz, IEEE Trans. Mag. **39** (5) (2003) 2950
- [21] S. N. Piramanayagam, M. Matsumoto, A. Morisako, S. Takei, J. Alloys Comp. **281**(1) (1998) 27
- [22] M. Yu, Y. Liu, S. H. Liou, D. J. Sellmyer, J. Appl. Phys. **83**(11) (1998) 6611
- [23] B. A. Kapitanov, N. V. Kornilov, Y. L. Linetsky, V. Y. Tsvetkov, J. Mag. Mag. Mat. **127**(3) (1993) 289
- [24] L. K. E. B. Serrona, A. Sugimura, N. Adachi, T. Okuda, H. Ohsato, I. Sakamoto, A. Nakanishi, M. Motokawa, D. H. Ping, K. Hono, Appl. Phys. Lett. **82** (2003) 1751
- [25] L. Castaldi, H. A. Davies, M. R. J. Gibbs, J. Mag. Mag. Mat. **242** (2002) 1284
- [26] A. S. Lileev, A. A. Parilov, V. G. Blatov, J. Mag. Mag. Mat. **242-245**(2) (2002) 1300

- [27] T. Shima, A. Kamegawa, K. Hono, H. Fujimori, *Appl. Phys. Lett.* **78** (2001) 2049
- [28] T. Okuda, A. Sugimura, O. Eryu, L. K. E. B Seronna, N. Adachi, I. Sakamoto, A. Nakanishi, *Jpn. J. Appl. Phys.* **42** (2003) 6859
- [29] F. J. Cadieu in: M. H. Francombe, J. L. Vossen (Eds.), *Physics of Thin Films*, Academic Press, Boston (1992) 145.
- [30] T. Budde, H. H. Gatzel, *J. Mag. Mag. Mat.* **242**(2) (2002) 1146
- [31] V. Neu, S. A. Shaheen, *J. Appl. Phys.* **86** (1999) 7006
- [32] F. J. Cadieu, R. Rani, T. Theodoropoulos, L. Chen, *J. Appl. Phys.* **85** (1999) 5895
- [33] V. Neu, J. Thomas, S. Fähler, B. Holzapfel, L. Schultz, *J. Magn. Magn. Mater.* **242-245** (2002) 1292
- [34] V. Neu, S. Fähler, B. Holzapfel, L. Schultz, 17th Int. Workshop on Rare-Earth Magnets and their Applications; Ed. G. C. Hadjipanayis, M. J. Bonder (Eds.), Rinton Press, Princeton (2002) 438
- [35] S. Leinert, V. Neu, S. Fähler, L. Schultz, in preparation.
- [36] E. E. Fullerton, J. S. Jiang, C. Rehm, C. H. Sowers, S. D. Bader, J. B. Patel, X. Z. Wu, *Appl. Phys. Lett.* **71** (1997) 1579
- [37] A. Singh, V. Neu, R. Tamm, S. Fähler, B. Holzapfel, W. Skrotzki, L. Schultz, *J. Appl. Phys.* (2004) submitted
- [38] T. Shima, K. Takanashi, Y. K. Takahashi, K. Hono, *Appl. Phys. Lett.* **81** (2002) 6
- [39] S. Fähler, S. Kahl, M. Weisheit, K. Sturm, H. U. Krebs, *Appl. Surf. Sci.* **154** (2000) 419
- [40] T. Suzuki, K. Harada, N. Honda, K. Ouchi, *J. Mag. Mag. Mat.* **193** (1999) 85-88
- [41] J. A. Christodoulides, M. J. Bonder, Y. Huang, Y. Zhang, S. Stoyanov, G. C. Hadjipanayis, A. Simopoulos, D. Weller, *Phys. Rev. B* **68** (2003) 054428
- [42] M. Weisheit, L. Schultz, S. Fähler, *J. Appl. Phys.* **95**(11) (2004) 7489
- [43] U. Hannemann, S. Melcher, S. Fähler, *J. Mag. Mag. Mat.* **272-276**(1) (2004) E859
- [44] R. F. C. Farrow, D. Weller, R. F. Marks, M. F. Toney, A. Cebollada, G. R. Harp, *J. Appl. Phys.* **79**(8) (1996) 5967
- [45] M. Weisheit, S. Fähler, unpublished work
- [46] M. R. Visokay, R. Sinclair, *Appl. Phys. Lett.* **66**(13) (1995) 1692
- [47] see e. g. K. Leister et al. and G. Zangari et al., these proceedings